JOC Article
pubs.acs.org/joc

Synthesis, Spectra, and Theoretical Investigations of the Triarylamines Based on 6*H*-Indolo[2,3-*b*]quinoxaline

K. R. Justin Thomas* and Payal Tyagi

Organic Materials Lab, Department of Chemistry, Indian Institute of Technology Roorkee, Roorkee 247 667, India

krjt8fcy@iitr.ernet.in

Received September 6, 2010

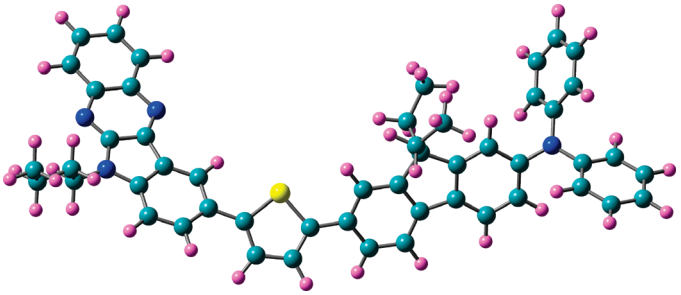

Triarylamines containing a 6*H*-indolo[2,3-*b*]quinoxaline core and aromatic units such as phenyl, naphthyl, pyrene, anthracene, or fluorene have been synthesized by employing palladium-catalyzed C−N and C−C coupling reactions and characterized by optical absorption and emission spectra, electrochemical behavior, and thermal studies. Even though the electronic absorption spectra of the compounds were influenced by the nature of the peripheral amines, the emission spectra indicated close similarity for the excited states in these compounds. For the derivatives in which the amines were directly anchored on the 6*H*-indolo[2,3-*b*]quinoxaline nucleus, the emission appeared to be dominated by the state localized on the 6*H*-indolo[2,3-*b*]quinoxaline chromophore, while in the compounds containing the extended conjugation the fluorescence originated from the polyaromatic linker. The compounds displayed green or yellow emission depending on the nature of the amine segment. All of the dyes displayed one-electron quasi-reversible oxidation couple in the cyclic voltammograms, which is attributable to the oxidation of the peripheral amines at the 6*H*-indolo[2,3-*b*]-quinoxaline core. An additional one-electron oxidation process observable at the high positive potentials for the compounds **7** and **8** probably arises from the oxidation of the arylthiophene segment. The enhanced thermal stability and relatively higher glass transition temperatures observed for these compounds were attributed to the presence of dipolar 6*H*-indolo[2,3-*b*]quinoxaline segment. The origin of the optical spectra and the trends observed therein were rationalized using TDDFT simulations.

Introduction

Organic semiconductors have received immense attention in recent years because of fundamental curiosity about their electro-optical properties and technological applications. In particular, the organic materials have been explored for use in electro-optical devices such as organic light-emitting diodes,[1] photovoltaics,[2] and organic field-effect transistors[3] on the basis of their functional efficacy. Molecules containing electron-donating amino groups have been found to exhibit interesting charge-transporting characteristics in electroluminescent devices.[4] Triarylamines featuring rigid

(1) (a) Tang, C. W.; VanSlyke, S. A. *Appl. Phys. Lett.* **1987**, *51*, 913. (b) Friend, R. H.; Gymer, R. W.; Holmes, A. B.; Burroughes, J. H.; Marks, R. N.; Taliani, C.; Bradley, D. D. C.; dos Santos, D. A.; Brédas, J. L.; Lögdlund, M.; Salaneck, W. R. *Nature* **1999**, *397*, 121. (c) Baldo, M. A.; Thompson, M. E.; Forrest, S. R. *Nature* **2000**, *403*, 750.

(2) (a) Grätzel, M. *Acc. Chem. Res.* **2009**, *42*, 1788. (b) Imahori, H.; Umeyama, T.; Ito, S. *Acc. Chem. Res.* **2009**, *42*, 1809. (c) Ning, Z.; Tian, H. *Chem. Commun.* **2009**, 5483.

(3) Anthony, J. E. *Angew. Chem., Int. Ed.* **2008**, *47*, 452.

(4) Shirota, Y. *J. Mater. Chem.* **2000**, *10*, 1.

Published on Web 11/05/2010 DOI: 10.1021/jo1016663

polyaromatic chromophores such as fluorene,[5] carbazole,[6] anthracene,[7] pyrene,[8] fluoranthene,[9] benzo[*k*]fluoranthene,[10] benzo[*a*]aceanthrylene,[11] dibenzothiophene,[12] perylene,[13] etc. have been developed for application in electronic devices as dual-functional materials possessing hole-transporting and fluorescent characteristics. Incorporation of rigid polyaromatic segments in the triarylamine core has been found to significantly enhance the emission and thermal properties.[6,14]

The color of the emission in such compounds was tuned by the electronic nature of the aromatic group. For instance, the fluorene-,[4] anthracene-,[7] and pyrene-based[8] triarylamines generally displayed blue emission, while the triarylamines derived from carbazole,[6] fluoranthene,[9] benzo[*k*]fluoranthene,[10] and perylene[13] ejected either green or yellow photons. It is probable that the introduction of polyaromatic groups in triarylamines extended the conjugation in the molecular structure, which effectively altered the physical properties such as absorption, emission, and thermal stability.[14] Extended conjugation is believed to result in intermolecular stacking interactions which are detrimental to the emission characteristics. However, the presence of bulkier groups around the trigonal amine nitrogen often hinders the aggregation of molecules in the solid state. The presence of fused polyaromatics such as pyrene, carbazole, fluoranthene, and benzo[*k*]fluoranthene in the triarylamine core has been found to be beneficial for the enhancement of thermal stability and glass transition temperature.[6,9,10] Additionally, the triarylamines derived from low band gap chromophores such as benzo[1,2,5]thiadiazole[15] and thieno[3,4-*b*]pyrazines[16] or electron-deficient units such as quinoxaline/pyrazine[17] and oxadiazole[18] exhibited balanced charge-transporting properties which were found to be important for the performance of electronic devices, particularly the organic light emitting diodes, photovoltaics, and thin film transistors.

Keeping the above-mentioned benefits of functional triarylamines in mind, we have recently initiated a research program to develop new molecular materials possessing dipolar structure built on the triarylamine core, featuring polyaromatic segments, and capable of displaying promising properties. In this paper, we present donor−acceptor compounds featuring indolo[2,3-*b*]quinoxaline segment and various diarylamines derived from anthracene, fluorene, or pyrene and their optical and electrochemical characteristics. The diarylamines are either directly anchored on the indoloquinoxaline segment through the indole nucleus or linked using a conjugating aromatic spacer. Inserting a spacer helps to modulate the electronic interaction between the amine unit and the indoloquinoxaline segment. Attempts were also made to understand the electronic structure of the newly synthesized molecules using TDDFT calculations. To the best of our knowledge, indoloquinoxaline-containing arylamines have not been reported previously, although indoloquinoxaline derivatives have been known in medicinal chemistry as antiviral and anticancer agents.[19] It has been observed that the indoloquinoxaline derivatives interact with DNA by the intercalation of the planar indolo[2,3-*b*]-quinoxaline moiety between the nucleobases. The indoloquinoxaline segment is a built-in donor−acceptor chromophore as it contains the electron-rich indole unit fused with the electron-deficient quinoxaline moiety. The electronic properties of the indoloquinoxaline segment can be altered by the introduction of electron-donating or electron-demanding groups on the indole as well as quinoxaline nucleus. The presence of electron-donating groups such as amines on the indole nucleus may enhance the donor ability of the indole moiety and increase the donor−acceptor interaction with the quinoxaline unit. Alternatively, addition of electron-accepting units may result in a bidirectional donor−acceptor interaction between the indole, quinoxaline, and auxiliary electron acceptors. Such a tunable molecular structure may be exploited for specific applications requiring donor−acceptor interactions and the resulting electronic properties.

Results and Discussion

Synthesis and Characterization. The synthesis of the indoloquinoxaline-based materials (Chart 1) was accomplished as illustrated in Scheme 1. The starting bromo derivative, 9-bromo-6-butyl-6*H*-indolo[2,3-*b*]quinoxaline, **2**,

(5) (a) Noine, K.; Pu, Y.-J.; Nakayama, K-.I.; Kido, J. *Org. Electron.* **2010**, *11*, 717–723. (b) Kwon, Y. S.; Lee, K. H.; Young, K. G.; Seo, J. H.; Kim, Y. K.; Yoont, S. S. *J. Nanosci. Nanotechnol.* **2009**, *9*, 7056–60. (c) Jiang, Z.; Liu, Z.; Yang, C.; Zhong, C.; Qin, J.; Yu, G.; Liu, Y. *Adv. Funct. Mater.* **2009**, *19*, 3987–3995. (d) Lai, M.-Y.; Chen, C.-H.; Huang, W.-S.; Lin, J. T.; Ke, T.-H.; Chen, L.-Y.; Tsai, M.-H.; Wu, C.-C. *Angew. Chem., Int. Ed.* **2008**, *47*, 581. (e) Gao, Z. Q.; Li, Z. H.; Xia, P. F.; Wong, M. S.; Cheah, K. W.; Chen, C. H. *Adv. Funct. Mater.* **2007**, *17*, 3194–3199. (f) Li, Z. H.; Wong, M. S.; Tao, Y.; Lu, J. *Eur. J. Chem.* **2005**, *11*, 3285. (g) Ego, B. C.; Grimsdale, F. U.; Yu, G.; Srdanov, G.; Müllen, K. *Adv. Mater.* **2002**, *14*, 809. (i) Loy, D. E.; Koene, B. E.; Thompson, M. E. *Adv. Func. Mater.* **2002**, *12*, 245.

(6) (a) Shen, J.-Y.; Yang, X.-L.; Huang, T.-H.; Lin, J. T.; Ke, T.-H.; Chen, L.-Y.; Wu, C.-C.; Yeh, M.-C. P. *Adv. Funct. Mater.* **2007**, *17*, 983. (b) Thomas, K. R. J.; Velusamy, M.; Lin, J. T.; Tao, Y.-T.; Chuen, C.-H. *Adv. Funct. Mater.* **2004**, *14*, 387. (c) Thomas, K. R. J.; Lin, J. T.; Tao, Y.-T.; Ko, C.-W. *J. Am. Chem. Soc.* **2001**, *123*, 9404.

(7) (a) Kim, S. K.; Yang, B.; Park, Y.-I.; Ma, Y.; Lee, J.-Y.; Kim, H.-J.; Park, J. *Org. Electron.* **2009**, *10*, 822. (b) Yang, B.; Kim, S. K.; Xu, H.; Park, Y.-I.; Zhang, H.-Y.; Gu, C.; Shen, F. Z.; Wang, C. L.; Liu, D. D.; Liu, X. D.; Hanif, M.; Tang, S; Li, W. J.; Li, F.; Shen, J. C.; Park, J. W.; Ma, Y.-G. *ChemPhysChem* **2008**, *9*, 2601. (c) Yu, M. X.; Duan, J. P.; Lin, C. H.; Cheng, C. H.; Tao, Y. T. *Chem. Mater.* **2002**, *14*, 3958. (d) Danel, K.; Huang, T.-H.; Lin, J. T.; Tao, Y.-T.; Chuen, C.-H. *Chem. Mater.* **2002**, *14*, 3860.

(8) (a) Thomas, K. R. J.; Velusamy, M.; Lin, J. T.; Chuen, C. H.; Tao, Y. T. *J. Mater. Chem.* **2005**, *15*, 4453–4459. (b) Jia, W.-L.; McCormick, T.; Liu, Q.-D.; Fukutani, H.; Motala, M.; Wang, R.-Y.; Tao, Y.; Wang, S. *J. Mater. Chem.* **2004**, *14*, 3344–3350.

(9) Kapoor, N.; Thomas, K. R. J. *New J. Chem.* **2010**, DOI: 10.1039/C0NJ00415D.

(10) Xia, Z. Y.; Su, J. H.; Fan, H. H.; Cheah, K. W.; Tian, H.; Che, C. H. *J. Phys. Chem. C* **2010**, *114*, 11602.

(11) Huang, T.-H.; Lin, J. T.; Tao, Y.-T.; Chuen, C.-H. *Chem. Mater.* **2003**, *15*, 4854.

(12) Huang, T.-H.; Lin, J. T.; Chen, L.-Y.; Lin, Y.-T.; Wu, C.-C. *Adv. Mater.* **2006**, *18*, 602.

(13) (a) Shen, W.-J.; Dodda, R.; Wu, C.-C.; Wu, F.-I.; Liu, T.-H.; Chen, H.-H.; Chen, C.-H.; Shu, C.-F. *Chem. Mater.* **2004**, *16*, 930. (b) Wu, C.-C.; Lin, Y.-T.; Chiang, H.-H.; Cho, T.-Y.; Chen, C.-W.; Wong, K.-T.; Liao, Y.-L.; Lee, G.-H.; Peng, S.-M. *Appl. Phys. Lett.* **2002**, *81*, 577.

(14) (a) Li, J.; Liu, D.; Li, Y.; Lee, C.-S.; Kwong, H.-L.; Lee, S. *Chem. Mater.* **2005**, *17*, 1208. (b) Kundu, P.; Thomas, K. R. J.; Lin, J. T.; Tao, Y.-T.; Chuen, C.-H. *Adv. Funct. Mater.* **2003**, *13*, 445.

(15) (a) Thomas, K. R. J.; Huang, T.-H.; Lin, J. T.; Pu, S.-C.; Cheng, Y.-M.; Hsieh, C.-C.; Chou, P.-T. *Chem.—Eur. J.* **2008**, *14*, 11231. (b) Thomas, K. R. J.; Lin, J. T.; Velusamy, M.; Tao, Y.-T.; Chuen, C.-H. *Adv. Funct. Mater.* **2004**, *13*, 83.

(16) Thomas, K. R. J.; Lin, J. T.; Tao, Y.-T.; Chuen, C.-H. *Adv. Mater.* **2002**, *14*, 822.

(17) (a) Thomas, K. R. J.; Lin, J. T.; Tao, Y.-T.; Chuen, C.-H. *Chem. Mater.* **2005**, *17*, 1860. (b) Thomas, K. R. J.; Lin, J. T.; Tao, Y.-T.; Chuen, C.-H. *Chem. Mater.* **2002**, *14*, 2796.

(18) Thomas, K. R. J.; Lin, J. T.; Tao, Y.-T.; Chuen, C.-H. *Chem. Mater.* **2004**, *16*, 5437.

(19) (a) Wilhelmsson, L. M.; Kingi, N.; Bergman, J. *J. Med. Chem.* **2008**, *51*, 7744. (b) Shibinskaya, M. O.; Lyakhov, S. A.; Mazepa, A. V.; Andronati, S. A.; Turov, A. V.; Zholobak, N. M.; Spivakm, N. Y. *Eur. J. Med. Chem.* **2010**, *45*, 1237–1243.

CHART 1. Structures of the Donor−Acceptor Compounds

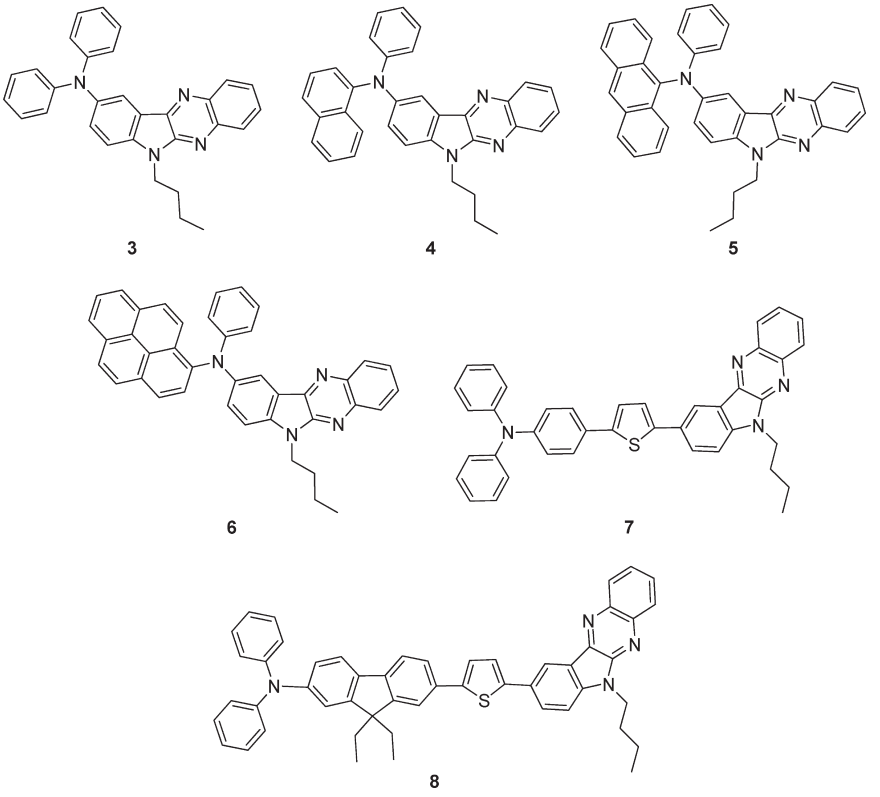

SCHEME 1. Synthesis of the Materials

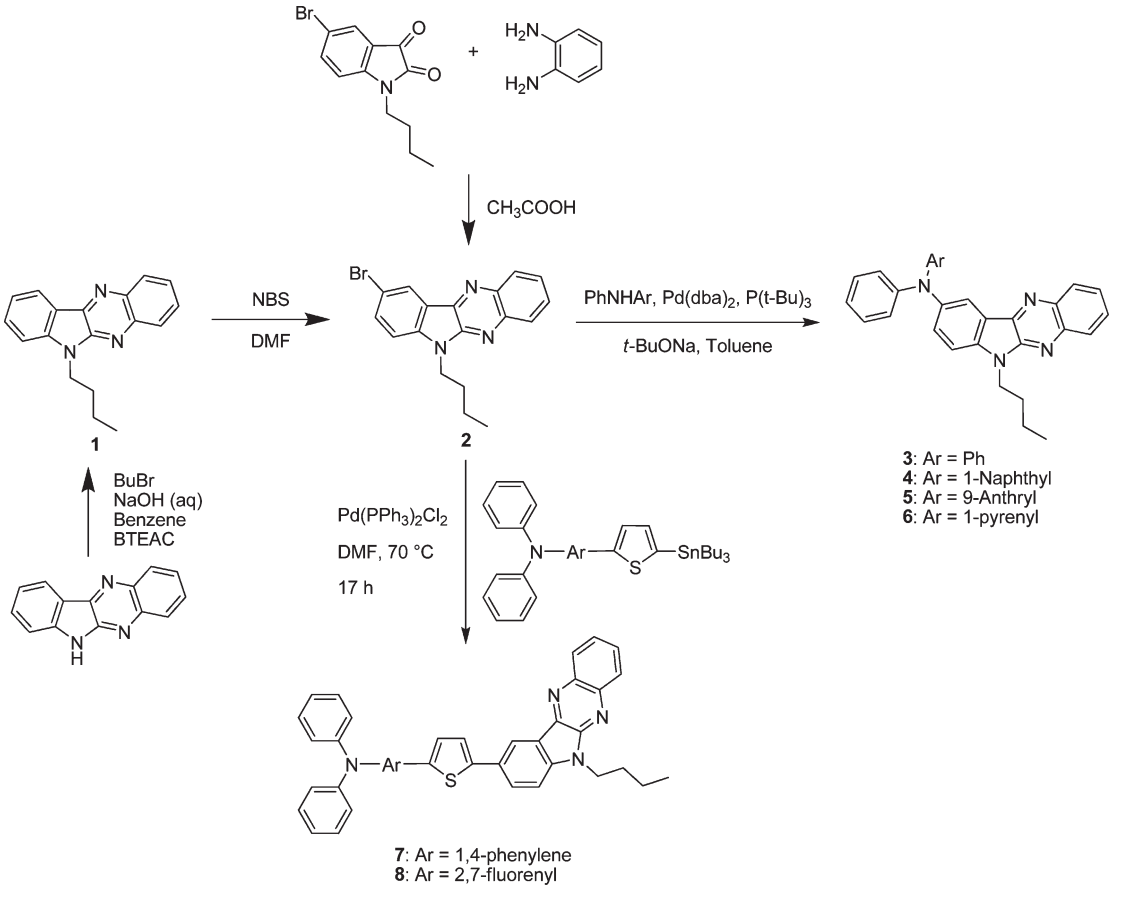

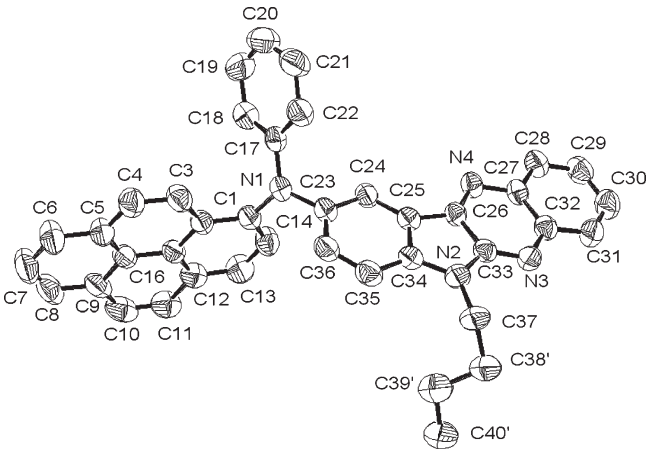

FIGURE 1. ORTEP plot (40% thermal ellipsoids, hydrogen atoms and the solvent molecule are omitted for clarity) of **6**.

required for the present study was acquired by following two different routes. In the first methody, the 6*H*-indolo[2,3-*b*]-quinoxaline was constructed from isatin and *o*-phenylenediamine and *N*-alkylated using *n*-butyl bromide and sodium hydroxide involving a phase-transfer catalysis protocol to obtain the 6-butyl-6*H*-indolo[2,3-*b*]quinoxaline. It was then brominated using *N*-bromosuccinimide to generate the desired precursor **2**. In an alternate procedure, the 5-bromo-1-butylindoline-2,3-dione was condensed with *o*-phenylenediamine in acetic acid to yield **2** in reasonable yield. Both methods produced identical compounds as confirmed by NMR spectroscopy and melting point measurements. The bromo precursor **2** was conveniently converted to the diarylaminated derivatives **3**−**6** by treating it with the corresponding diarylamine in the presence of $Pd(dba)_2$, $P(t\text{-}Bu)_3$, and sodium *tert*-butoxide. The compounds (**7** and **8**) containing conjugation between the peripheral amino unit and indoloquinoxaline segment were easily obtained by following the Stille coupling reaction between **2** and the suitable tin reagents. All of the target compounds (**3**−**8**) are deep orange or red solids soluble in common organic solvents including dichloromethane, toluene, acetonitrile, etc. However, they are only sparingly soluble in alcohols and insoluble in water. The structural compositions of the compounds were established by spectral (^{1}H, ^{13}C NMR and high-resolution mass) methods and elemental analysis. In addition, the structure of compound **6** was confirmed by single-crystal X-ray diffraction analysis (vide supra).

Structural Analysis of 6. Crystals of the compound **6** were grown from dichloromethane/hexane mixture at room temperature. The monoclinic crystals assumed the $P2_1/n$ space group and included a solvent molecule in the crystal lattice. The solvent and the butyl chain were found to be disordered. The ORTEP representation of **6** is shown in Figure 1 (The CH_2Cl_2 molecule and the disordered butyl group were omitted for clarity). The important bond angles and bond distances are collected in Tables 1. The three aromatic segments, viz. phenyl (P1), pyrene (P2), and indoloquinoxaline (P3), are assuming non-coplanar arrangement due to the trigonal geometry adopted by the amine nitrogen. The dihedral angles observed for the P1/P2, P2/P3, and P1/P3 pairs are 70.13°, 89.85°, and 76.89°, respectively. The twist of these aromatic rings from the coplanarity disfavors the intermolecular $\pi-\pi$ stacking interactions even from the units of adjacent molecules. The bond

TABLE 1. Selected Bond Lengths (Å) and Angles (deg) for 6

bond length (Å)		bond angles (deg)	
N(1)−C(1)	1.428(4)	C(24)−C(23)−N(1)	121.2(4)
N(1)−C(17)	1.398(5)	C(36)−C(23)−N(1)	118.5(3)
N(1)−C(23)	1.429(5)	N(2)−C(37)−C(38)	106.8(4)
N(2)−C(33)	1.365(5)	C(39)−C(38)−C(37)	105.1(8)
N(2)−C(34)	1.391(5)	C(38)−C(39)−C(40)	111.2(12)
N(2)−N(37)	1.450(5)	C(17)−N(1)−C(1)	122.5(3)
C(37)−C(38)	1.533(5)	C(17)−N(1)−C(23)	119.6(3)
C(38)−C(39)	1.512(5)	C(1)−N(1)−C(23)	115.8(3)
C(39)−C(40)	1.524(5)	C(33)−N(2)−C(37)	124.9(3)
		C(34)−N(2)−C(37)	126.3(3)

distance N(1)−C(17) is slightly shorter (1.398(5) Å) than the average value observed for the arylamines (1.420 Å); however, the bond angle C(17)−N(1)−C(23), 119.6(3)°, is quite close to the average value of 119.99.[20] From the shorter N−C bond it may speculated that the lone-pair electrons on the nitrogen are more delocalized into the phenyl ring rather than the pyrene and indoloquinoxaline segments. An antistaggered conformation was observed for the *n*-butyl chain present in the indolo-[2,3-*b*]quinoxaline moiety.

There are no van der Waals intermolecular interactions between the CH_2Cl_2 solvent and **6**, but there are weak hydrogen-bonding interactions between the pyrene and indoloquinoxaline segments as depicted in Figure 2. The C−H−π interactions observed between the phenyl ring of the 6-butyl-6*H*-indolo[2,3-*b*]quinoxaline moiety and the pyrene are in the range of 2.75−2.84 Å and with a C−H···π angle are in the range of 148.8−158.8°. These values are in close agreement with the literature-reported H···π distance of 2.8−2.9 Å and C−H···π angle of 152−159°.[21] A notable hydrogen-bonding interaction between the nitrogen atom of the quinoxaline and a hydrogen of pyrene is observed with a distance of 2.73 Å and N···H−C angle of 145.7°. This is also in accordance with the experimentally observed average N···H distance (2.8−2.9 Å)[22] and the theoretically predicted values (2.68−3.06 Å).[23] However, N···H−C angles observed in the literature are in the wide range of 120−180°. It is probable that the stabilization of the crystal **6** in the solid state is facilitated by the weak C−H−π and N···H−C hydrogen-bonding interactions.

Photophysical Studies. The absorption spectra of the compounds were measured in dichloromethane. The pertinent data are listed in Table 2 and the spectral profiles displayed in Figure 3. Compounds **3**−**8** exhibited multiple bands originating from different $\pi-\pi^*$ and charge-transfer transitions.

The absorption spectra of the compounds are dominated by multiple overlapping bands owing to the presence of different nonconjugated chromophoric segments. The electronic spectra of the parent compound **1** possess two bands arising from the $\pi-\pi^*$ (λ_{max} = 355 nm) and charge-transfer

(20) Wang, B. C.; Liaoa, H.-R.; Chang, J.-C.; Chen, L.; Yeh, J.-T. *J. Lumin.* **2007**, *124*, 333.
(21) (a) Yoon, I. I.; Benítez, D.; Miljanic, O. S.; Zhao, Y.-L.; Tkatchouk, E.; Goddard, W. A.; Stoddart, J. F. *Cryst. Growth Des.* **2009**, *9*, 2300. (b) Baez, E. V. G.; Martinez, F. J. M.; Hopfl, H.; Martinez, I. I. P. *Cryst. Growth Des.* **2003**, *3*, 35. (c) Thalladi, V. R.; Gehrke, A.; Boese, R. *New J. Chem.* **2000**, *24*, 463. (d) Thalladi, V. R.; Smolka, T.; Gehrke, A.; Boese, R.; Sustmann, R. *New J. Chem.* **2000**, *24*, 143.
(22) Thaimattam, R.; Reddy, D. S.; Xue, F.; Mak, T. C. W.; Nangia, A.; Desiraju, G. R. *J. Chem. Soc., Perkin Trans. 2* **1998**, 1783.
(23) Domagala, M.; Grabowski, S. J. *J. Phys. Chem. A* **2005**, *109*, 5683.

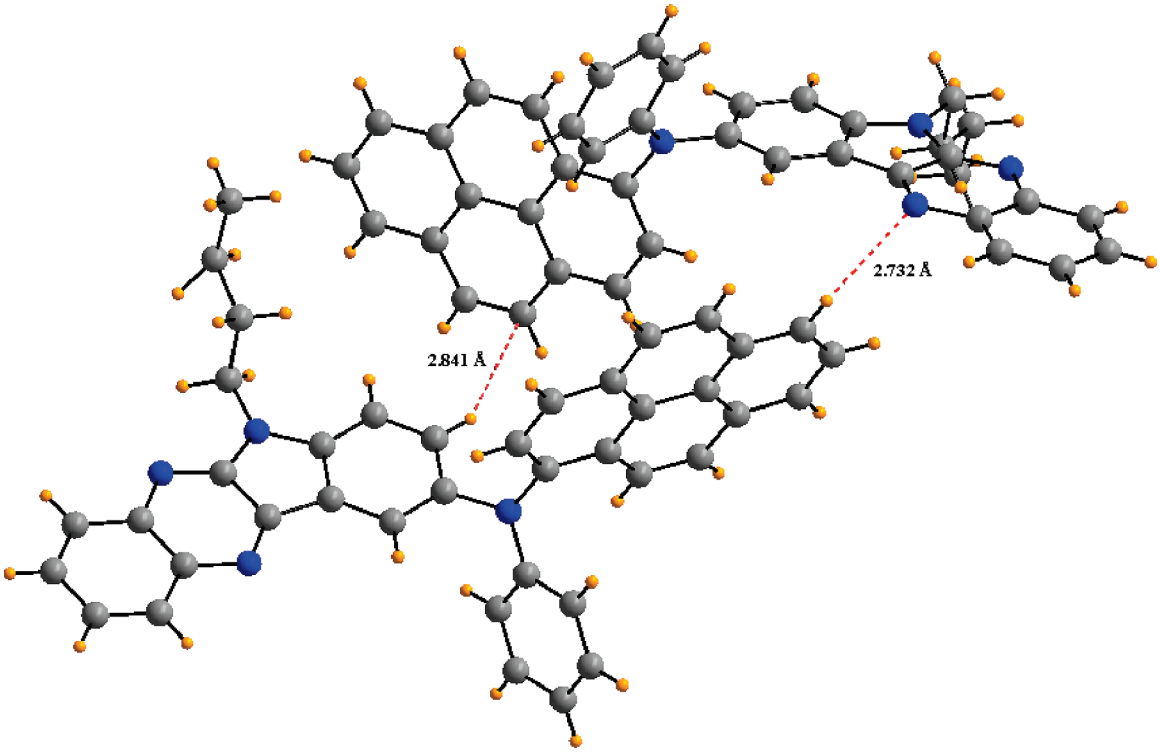

FIGURE 2. Illustrations of C−H···π and N···H−C interactions in the crystal of **6**.

TABLE 2. Photophysical Parameters Observed for the Compounds

compd	λ_{max} (nm) (ε_{max}, M^{-1} cm^{-1} × 10^3)[a]	λ_{max}(nm) (ε_{max}, M^{-1} cm^{-1} × 10^3)[b]	λ_{em}(nm) (Φ_f)[b,c]	Stokes shift[d] (cm^{-1})	E_{0-0}[e] (eV)
3	262 (41.5), 312 (45.9), 377 (19.8), 447 (1.3)	311 (35.4), 359 (14.4), 377 (16.9), 447 (1.3)	578 (0.01)	5070	2.38
4	262 (44.1), 316 (37.8), 358 (23.0), 376 (25.6), 455 (1.3)	317 (31.3), 358 (20.7), 377 (25.3), 455 (1.4)	579 (0.08)	4707	2.38
5	255 (80.5), 326 (52.1), 381 (15.0), 426 (8.5)	327 (51.3), 382 (15.6), 422 (8.8)	586 (0.01)	6632	2.38
6	262 (52.2), 271 (46.6), 317 (43.7), 379 (24.5), 412 (13.7)	318 (35.2), 379 (20.2), 408 (12.6)	584 (0.01)	7387	2.38
7	264 (36.3), 308 (28.9), 371 (56.2)	309 (32.9), 374 (62.9)	553 (0.01)	8655	2.43
8	263 (46.5), 295 (35.1), 390 (83.8)	296 (20.5), 392 (47.4)	544 (0.02)	7127	2.43

[a]Measured in dichloromethane. [b]Measured in toluene. [c]Quantum yield with reference to coumarin **6** (0.78 = in ethanol). [d]Calculated from the absorption and emission wavelengths observed in toluene. [e]Calculated from the optical edge estimated for the dichloromethane solutions.

(CT) (λ_{max} = 405 nm) transitions, respectively. The former band exhibits a characteristic vibronic pattern. This higher energy transition is attributed to the $\pi-\pi^*$ transition originating from the entire indoloquinoxaline unit. The lower energy transition may be due to charge transfer between the electron-donating indole and the electron-accepting quinoxaline units. The dyes **3**−**8** display a prominent band >370 nm which is analogous to the first band in the precursor **1** but more red-shifted than in **1**. The red-shift is justified considering the auxochromic effect exerted by the amine unit. The second band is slightly red-shifted in the diphenylamine and 1-naphthylphenylamine derivatives **3** and **4** when compared to that in **1** with a concomitant reduction in the intensity. It is expected that the electron-donating diarylamine would enhance the donor ability of the indole segment and enhance the charge transfer between the indole and quinoxaline segments, but the observed decrease in the absorbance indicates that the transition probability for this charge transfer reduces upon substitution of amines on the indole segment. In place of this peak, there exists a slightly intense band in the spectra of the anthracene and pyrene derivatives (**5** and **6**). These transitions are attributed to the anthracenamine[7] and pyrenamine-based[6,8] electronic excitations. A new band at λ_{max} = 320 nm was observed in all of the dyes when compared to **1**, which is attributed to $\pi-\pi^*$ transition located within the arylamine units. In addition, an $n-\pi^*$ transition originating from the terminal arylamine moiety is also expected to appear at ~300 nm or below, and it is probably overlapping with the intense $\pi-\pi^*$ transitions.

Among the dyes **3**−**6**, the pyrene derivative **6** shows an intense charge-transfer band caused by the comparatively strong π-accepting nature of the pyrene. This also suggests that the charge-transfer transition for this compound (**6**) may have contributions from amine to pyrene transition. The absorption spectra of compounds **7** and **8** indicate a bathochromic shift and a hyperchromism for the $\pi-\pi^*$ transition when compared to the other derivatives containing a diarylamine segment directly attached to the indole

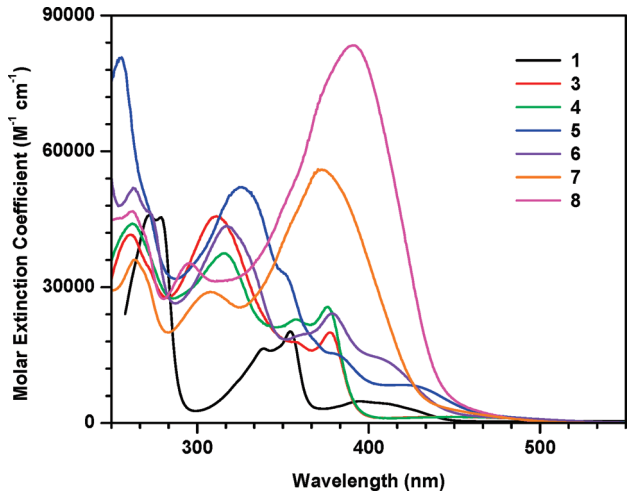

FIGURE 3. Absorption spectra of the compounds (**1** and **3**−**8**) recorded for dichloromethane solutions.

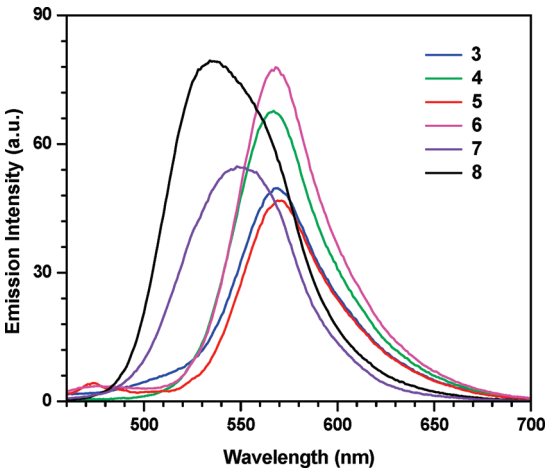

FIGURE 4. Emission spectra of the compounds (**3**−**8**) recorded in toluene.

nucleus (**3**−**6**). In compounds **7** and **8**, the $\pi-\pi^*$ transition originates mainly from the aromatic side chain and shows a broad peak due to the merger of the indoloquinoxaline-based $\pi-\pi^*$ transition. This assignment is reasonable when considering the asymmetric broadening in the absorption profile of these dyes, which indicates the presence of two or more overlapping peaks.

All of the compounds with the exception of **7** and **8** emit pale orange light when excited at 420 nm in toluene (Figure 4), yet a blue-shifted yellow emission was witnessed for compounds **7** and **8**. The emission peak of the amine derivatives **3**−**6** was less sensitive to the nature of the diarylamine tethered to the indole nucleus, while in **7** and **8** the emission profile reflects the effect due to the alternation in the nature of the conjugation bridge. This clearly indicates that the origin of emission in the compounds arises from different locations. For the amine derivatives **3**−**6**, it probably originates from the indoloquinoxaline-based excited state, and the excitation at the peripheral amine segment leads to the efficient energy migration to the indoloquinoxaline reservoir. However, in compounds **7** and **8**, the fluorescence originates from the peripheral aromatic linkage rather than the chromophore comprising the indoloquinoxaline segment. The relatively low quantum yields observed for the compounds even in toluene suggest a prominent nonradiative deactivation pathway for the excited state. In addition to the vibrational relaxation, the excited state of a luminophore may be quenched by several physical processes such as photoinduced electron transfer, resonance energy transfer to a quencher, dipole−dipole interaction, complex formation, etc. More pronounced emission quenching observed in the polar solvents such as dichloromethane, acetonitrile, and tetrahydrofuran indicates the presence of dipole−dipole interactions.

Electrochemical Studies. The charge-transport capability of a material can be identified from its propensity to stabilize both cation and anions. Electrochemical measurements can be used to estimate the capability of the dyes to produce and stabilize the cations and anions. We have studied the newly synthesized molecules by cyclic voltammetric and differential pulse voltammetric measurements in dichloromethane with 0.1 M tetrabutylammonium hexafluorophosphate as the electrolyte in a conventional three-electrode assembly. Ferrocene was used as an internal standard to calibrate the redox potentials. The observed parameters are reported in Table 3. Selected cyclic voltammograms are displayed in Figure 5.

All of the dyes displayed one-electron quasi-reversible oxidation couple at the relatively low oxidation potentials, which is more positive than that observed for ferrocene. It is attributable to the oxidation of the peripheral amines at the 9-position of the 6*H*-indolo[2,3-*b*]quinoxaline core as there is no oxidation wave observed for the parent core in this region. The oxidation potential increases in the following order: **5** < **8** < **6** < **7** < **3** < **4**. This trend is attributable to the electron-donating nature of the aryl substituents attached to the amine nitrogen. Among the diphenylamine containing dyes the oxidation potential assumes the following order: **3** > **7** > **8**. This is in keeping with the difference in the electron richness of the aromatic linker segments (phenylthiophene vs thienylfluorene). Thiophene[24] and fluorene-containing[5] arylamines have been reported to exhibit facile oxidation owing to the electron richness of the thiophene and fluorene moieties. Additionally, it is possible that the insertion of polyaromatic spacers between the amine and indoloquinoxaline moieties may decrease the electronic communication between them as the distance between the amine donor and the electron-accepting quinoxaline segment increases.[25]

An additional one-electron oxidation at the high positive potential is also observed for the compounds **7** and **8**, which probably stems from the aromatic conjugation pathway caused by the presence of the electron-rich thiophene segment. It is cathodically shifted for the thienylfluorene-containing dye **8** owing to the electron richness of the fluorene when compared to the compound (**7**) containing the thienylphenyl segment.[26] An irreversible reduction arising from the quinoxaline segment was also observed for all the dyes. Quinoxalines display facile reversible reduction couple when

(24) Thomas, K. R. J.; Lin, J. T.; Tao, Y.-T.; Ko, C.-W. *Chem. Mater.* **2002**, *14*, 1354.
(25) Thomas, K. R. J.; Lin, J. T.; Tao, Y.-T.; Chuen, C.-H. *J. Mater. Chem.* **2002**, *12*, 3516.
(26) (a) Chen, C.-H.; Hsu, Y.-C.; Chou, H.-H.; Thomas, K. R. J.; Lin, J. T.; Hsu, C.-P. *Chem.—Eur. J.* **2010**, *16*, 3184. (b) Yen, Y.-S.; Hsu, Y.-C.; Lin, J. T.; Chang, C.-W.; Hsu, C.-P.; Yin, D.-J. *J. Phys. Chem. C* **2008**, *112*, 11557. (c) Thomas, K. R. J.; Lin, J. T.; Hsu, Y.-C.; Ho, K.-C. *Chem. Commun.* **2005**, 4098.

TABLE 3. Electrochemical and Thermal Data of the Dyes

compd	E_{ox}, V (ΔE_p, mV)[a]	HOMO[b] (eV)	LUMO[c] (eV)	T_d (onset)[d] (°C)	T_g (°C)	T_m (°C)
3	0.367 (68)	5.17	2.79	578 (383)	NA	188
4	0.395 (51)	5.20	2.82	579 (445)	74	175
5	0.312 (74)	5.11	2.73	586 (416)	94	238
6	0.337 (69)	5.14	2.76	584 (439)	110	161
7	0.342 (59), 0.623 (68)	5.14	2.71	553 (441)	85	218
8	0.331 (55), 0.592 (65)	5.13	2.70	544 (469)	104	195

[a]Obtained from cyclic voltammograms. Potentials reported are referenced related to the ferrocene internal standard. [b]Derived from the oxidation potential using $E_{HOMO} = 4.8 + E_{ox}$. [c]Deduced using the formula $E_{LUMO} = E_{HOMO} - E_{0-0}$; [d]Measured in air, heating rate 10 °C/min.

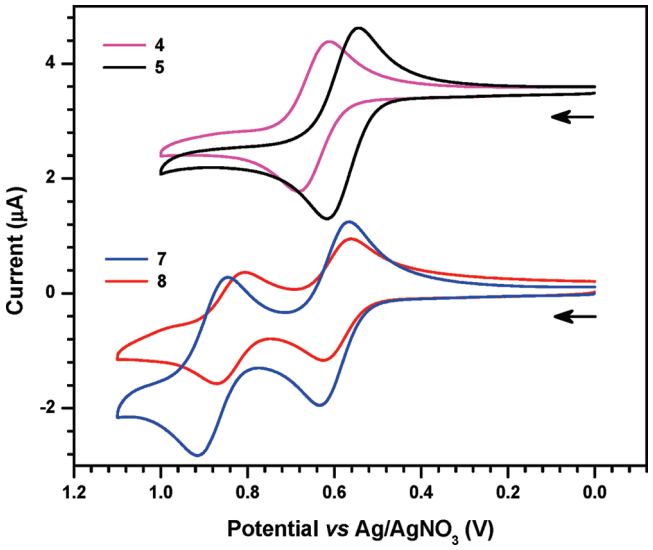

FIGURE 5. Cyclic voltammograms recorded for the compounds in dichloromethane (conditions, ~2.5×10^{-5} M solutions; scan rate, 100 mV/s; electrolyte, tetrabutylammonium hexafluorophosphate).

attached to the electron-withdrawing groups.[17] Observation of irreversible reduction for the present dyes suggests the electron-donating role of indole and the amine segments. They probably reduce the electron affinity of the quinoxaline unit. Consequently, the reduction potential shifts cathodically on increasing the donor strength of the amine.

The HOMO and LUMO energy levels of the materials are very crucial parameters for most of the electro-optical devices, which guides the interfacial charge transport kinetics. The HOMO energy levels of the compounds (Table 3) were calculated using the formula HOMO = (E_{ox} + 4.8) from the first oxidation potential by comparison with ferrocene (4.8 eV) of those ranges from 5.11 to 5.20 eV. The HOMO energy levels of the dyes are slightly lower than that of the most widely used hole-transport material 4,4′-bis(1-naphthylphenylamino)-biphenyl (NPB) (HOMO = 5.20 eV; LUMO = 2.4 eV) and thus might be beneficial for the hole injection and transport property.[27] Similarly, the lowest unoccupied molecular orbital (LUMO) levels were estimated from the values of HOMO and the band gap (E_{0-0}) by using the equation LUMO = HOMO − E_{0-0}. The band gaps of the compounds were estimated from the optical edge. The energy gap $E_{0-0,}$ for the thiophene-linked compounds (**7** and **8**) is smaller than that of **3**, owing to the electron-releasing effect of the thiophene and/or longer conjugation. Among the dyes, the anthracene- (**5**) and pyrene-containing (**6**) derivatives possess lower LUMO probably due to relatively good π-accepting ability of the anthracene and pyrene units. The presence of electron-withdrawing groups such as CF_3, CN, etc. has been demonstrated to stabilize the LUMO in molecular materials.[6b,18] Similarly, in a series of analogous compounds the anthracene and pyrene compounds possessed low-lying LUMO when compared to the compounds featuring phenyl and naphthyl units.[6b] It is interesting to compare the orbital energies reported previously in the literature for the anthracene-bridged triarylamines such as 9,10-bis(diphenylamino)anthracene (PPA)[7c] and 9,10-bis(1-naphthylphenylamino)anthracene (NPA)[7c] with the present compounds and related triarylamines containing linkers such as phenyl, biphenyl, or fluorene. It is clearly evident that the nature of the aryl substituents in the triarylamine unit significantly alters the HOMO/LUMO energies. For instance, the above-mentioned anthracene-containing derivatives PPA and NPA possess the low-lying LUMO levels at 3.2 and 3.1 eV, respectively, when compared to the other derivatives. It appears that the polynuclear aromatics being good π-acceptors probably stabilize the LUMO. The variations in the HOMO and LUMO energies observed in the present series of compounds arise mainly from the alterations in the π-acceptor ability and the σ-donor strength of the aryl substituents either acting as the linkers or present in the peripheral amines.

Thermal Investigations. The thermal properties of the dyes were examined by both thermogravimetric analysis and differential scanning calorimetry. The thermal decomposition temperatures, melting points, crystallization temperatures, and glass transition temperatures observed for the dyes are listed in Table 3. All of the compounds with the exception of **3** are amorphous in nature as evidenced by their high glass transition temperature. They showed melting endotherms in the first heating cycle but on rapid cooling of the melt led to the formation of a glassy state which persisted in the subsequent heating cycles. Compounds **3** and **4** also showed crystallization exotherms on cooling in the first cycle; however, such behavior is not observed with the other compounds.

All of the compounds exhibit moderate glass transition temperatures in the range 75−110 °C, which is comparable to those recorded for the commonly used hole-transporting agents such as 1,4-bis(phenyl-*m*-tolylamino)biphenyl (TPD, T_g = 60 °C) and 4,4′-bis(1-naphthylphenylamino)biphenyl (NPB, T_g = 95 °C).[27b] The pronounced stability of the glassy state in these molecules is attributed to the nonplanar molecular configurations arising from the steric hindrance of the bulky secondary amines and polar structural elements. Pyrenylphenylamine derivative **6** possesses the highest glass transition temperature in the series as the rigid and flat pyrene tends to hinder translational, rotational, and vibrational motions of the

(27) (a) Wu, C.; Djurovich, P. I.; Thompson, M. E. *Adv. Func. Mater.* **2009**, *19*, 3157. (b) Koene, B. E.; Loy, D. E.; Thompson, M. E. *Chem. Mater.* **1998**, *10*, 2235.

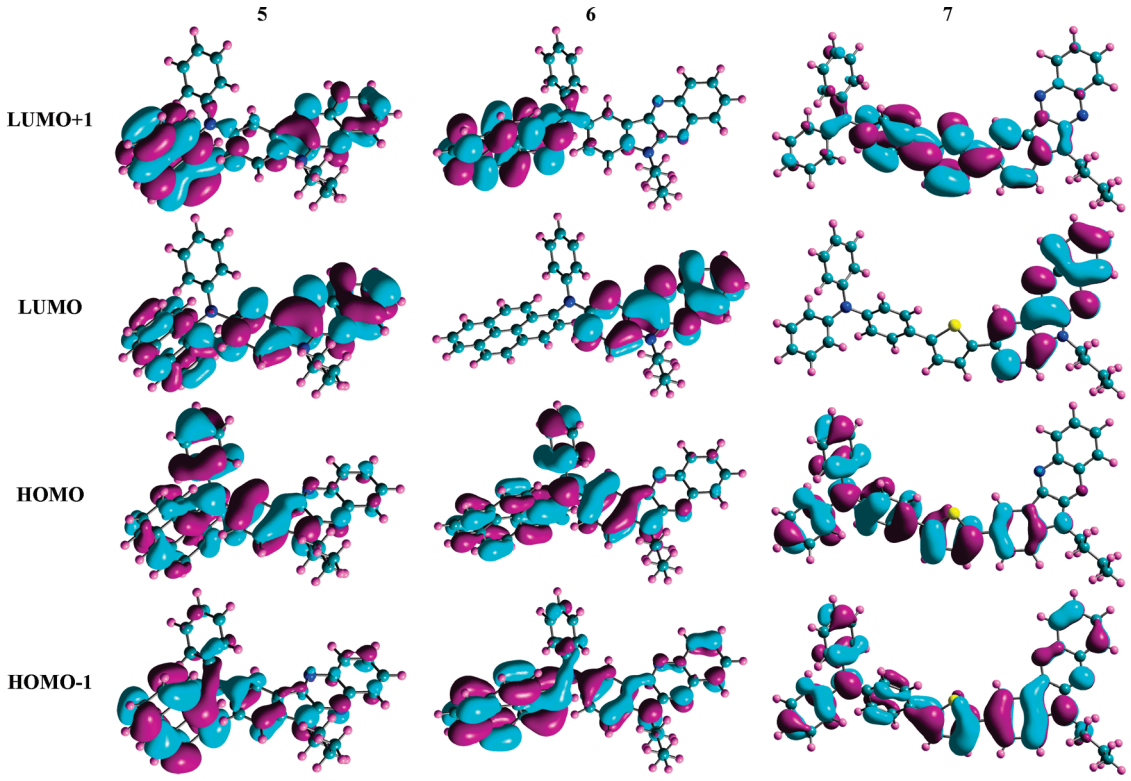

FIGURE 6. Frontier orbitals of the derivatives **5**, **6**, and **7**.

molecule and result in T_g enhancement.[14,28] Insertion of thiophene in the conjugation pathway leads to a significant enhancement in the T_g, which is probably triggered by the enhanced rigidity and elongated conjugation. Upon comparison of the phenylenethiophene (**7**) and thienylfluorene (**8**) derivatives, observation of lower T_g for the fluorene derivative is attributed to the flexible *n*-alkyl moieties present in the latter compound.[29]

The thermal stability of these materials also seems to be encouraging. The thermal decomposition temperatures of these materials occur above 380 °C in air. Within the class, the dye-containing diphenylamine donor (**3**) displays lower thermal decomposition temperature when compared to the naphthalene, anthracene, and pyrene containing dyes **4**−**6**. The order of the thermal stability among the diarylamine derivatives is **3** < **4** < **5**−**6**. Enhancement of the glass transition temperature for the compounds bearing the polyaromatics such as naphthalene, anthracene, and pyrene has been previously observed and is attributed to the increased rigidity on incorporation of polyaromatics.[27b] In general, the compounds containing diarylamine directly attached to the indoloquinoxaline core (**3**−**6**) surpass in thermal stability the compounds in which the diarylamine is separated by a polyaromatic linker (**7** and **8**).

The beneficial role of indolo[2,3-*b*]quinoxaline for raising the thermal decomposition temperature (544−586 °C) and glass transition temperature (74−110 °C) of these materials is clearly evident when compared with the previously reported hole-transporting materials such as PPA, NPA, TPD, and NPB.[7c,27b] They exhibit a moderate thermal stability (185−382 °C) despite having two end-capping diarylamine segments. The high thermal stability and glass transition temperature observed for the present dyes may be attributed to the planar arrangement of the indolo[2,3-*b*]quinoxaline moiety, which provides additional rigidity to the molecule. It is also worth mentioning that the enhanced thermal stability and high glass transition temperatures of the dyes will be beneficial for the fabrication of amorphous thin films.

Theoretical Investigations. To gain insight into the electronic structure of the dyes, TDDFT calculations were performed on the dyes using the Gaussian 09 package.[30] The atomic coordinates obtained from the crystal structure were used as the initial guess structure and optimized fully by the DFT in the gas state. Other molecules were similarly optimized by modifying the aryl substituent suitably. Electronic calculations were performed using B3LYP as an exchange-correlation functional and 6-31G(d,p) basis set.

Figure 6 shows the theoretically computed molecular orbitals in the ground states for the representative compounds **5**−**7**. In all of the compounds, the HOMO and

(28) (a) Noda, T.; Imae, I.; Noma, N.; Shirota, Y. *Adv. Mater.* **1997**, *9*, 239. (b) O'Brien, D. F.; Burrows, P. E.; Forrest, S. R.; Koene, B. E.; Loy, D. E.; Thompson, M. E. *Adv. Mater.* **1998**, *10*, 1108.

(29) Kreger, K.; Jandke, M.; Strohriegl, P. *Synth. Met.* **2001**, *119*, 163.

(30) Gaussian 09, Revision A.1. Frisch, M. J.; Trucks, G. W.; Schlegel, H. B.; Scuseria, G. E.; Robb, M. A.; Cheeseman, J. R.; Scalmani, G.; Barone, V.; Mennucci, B.; Petersson, G. A.; Nakatsuji, H.; Caricato, M.; Li, X.; Hratchian, H. P.; Izmaylov, A. F.; Bloino, J.; Zheng, G.; Sonnenberg, J. L.; Hada, M.; Ehara, M.; Toyota, K.; Fukuda, R.; Hasegawa, J.; Ishida, M.; Nakajima, T.; Honda, Y.; Kitao, O.; Nakai, H.; Vreven, T.; Montgomery, J. A., Jr.; Peralta, J. E.; Ogliaro, F.; Bearpark, M.; Heyd, J. J.; Brothers, E.; Kudin, K. N.; Staroverov, V. N.; Kobayashi, R.; Normand, J.; Raghavachari, K.; Rendell, A.; Burant, J. C.; Iyengar, S. S.; Tomasi, J.; Cossi, M.; Rega, N.; Millam, N. J.; Klene, M.; Knox, J. E.; Cross, J. B.; Bakken, V.; Adamo, C.; Jaramillo, J.; Gomperts, R.; Stratmann, R. E.; Yazyev, O.; Austin, A. J.; Cammi, R.; Pomelli, C.; Ochterski, J. W.; Martin, R. L.; Morokuma, K.; Zakrzewski, V. G.; Voth, G. A.; Salvador, P.; Dannenberg, J. J.; Dapprich, S.; Daniels, A. D.; Farkas, O.; Foresman, J. B.; Ortiz, J. V.; Cioslowski, J.; Fox, D. J. Gaussian, Inc., Wallingford CT, 2009.

TABLE 4. Computed Ionization Potentials, Electron Affinities, Vertical Excitations, Dipole Moments, and Orbital Energies

compd	I_p (eV)	E_a (eV)	λ_{max} (nm)	f	assignment	μ_g (debye)	HOMO (eV)	LUMO (eV)	E_g (eV)
3	−5.94	0.69	510.5	0.0095	HOMO→LUMO (99%)	2.30	−4.84	−1.90	2.94
			361.7	0.0464	HOMO−1→LUMO (94%)				
4	−5.90	0.68	498.8	0.0101	HOMO → LUMO (99%)	2.54	−4.88	−1.88	3.00
			392.0	0.1423	HOMO→LUMO+1 (98%)				
5	−5.84	0.87	511.2	0.0472	HOMO→LUMO (80%)	2.77	−4.83	−1.88	2.95
					HOMO→LUMO+1 (17%)				
			497.8	0.0338	HOMO→LUMO+1 (80%)				
					HOMO→LUMO (18%)				
			396.1	0.0563	HOMO−1→LUMO (96%)				
			380.2	0.0640	HOMO−1→LUMO+1 (94%)				
6	−5.77	0.83	510.8	0.0091	HOMO→LUMO (98%)	2.43	−4.80	−1.89	2.91
			447.7	0.3146	HOMO→LUMO+1 (95%)				
7	−5.67	0.74	491.3	0.0106	HOMO→LUMO (95%)	2.26	−4.79	−1.92	2.87
			405.4	0.0538	HOMO−1→LUMO (91%)				
			396.8	1.2097	HOMO→LUMO+1 (97%)				
8	−5.57	0.81	488.1	0.0104	HOMO→LUMO (91%)	2.17	−4.75	−1.93	2.82
					HOMO−1→LUMO (9%)				
		425.7	0.0324		HOMO−1→LUMO (87%)				
					HOMO→LUMO (9%)				
		413.8	1.3277		HOMO→LUMO+1 (96%)				

LUMO are mainly constituted by the triarylamine including the indole nucleus and the indoloquinoxaline segments, respectively, with the exception of the anthracene derivative **5**. In the case of the anthracene derivative (**5**), the LUMO is spread over the anthracene as well. This explains the substantial stabilization of LUMO in the compound **5** as revealed by the electrochemical and optical studies (vide supra). The location of HOMO/LUMO orbitals on the donor/acceptor moieties has been commonly observed in the molecules featuring donor−acceptor architecture[31] and is considered an indication of the prominent absorption, HOMO to LUMO electronic transition, originating from a charge transfer state. However, for the present compounds the charge-transfer transition is characteristic of a forbidden one and possesses invariably small oscillator strength for all of the dyes studied in this work (vide supra).

The energies of the HOMO and LUMO levels, HOMO−LUMO gap, first ionization potential, electron affinity, and ground-state dipole moment computed for the dyes **3**−**8** are collected in Table 4. The HOMO and LUMO energy levels of the compounds occur in the narrow ranges 4.75−4.88 and 1.88−1.93 eV, respectively. The HOMO−LUMO gap of the dyes ranged 2.82−3.0 eV and slightly decreased on the extension of the conjugation pathway between the amine donor and the indoloquinoxaline segments. The LUMO energies and the energy gap calculated for the dyes in the gas phase significantly deviated from the values deduced from optical edge and electrochemical measurements, which probably indicate a role of solvent interaction with the molecules. The observed/calculated LUMO values suggest that these compounds may not be effective as electron-transport layers as there may be a significant energy barrier for the electron injection from the cathode. On the contrary, the favorable HOMO values predict a facile hole injection from the anode (for instance, ITO) having a work function of ~4.8 eV. The adiabatic ionization potential and electron affinity computed for the dyes are also in agreement with the above observations. Electron-rich triarylamines and extension of conjugation reduce the ionization energy.

(31) Zhu, Y.; Kulkarni, A. P.; Wu, P.-T.; Jenekhe, S. A. *Chem. Mater.* **2008**, *20*, 4200.

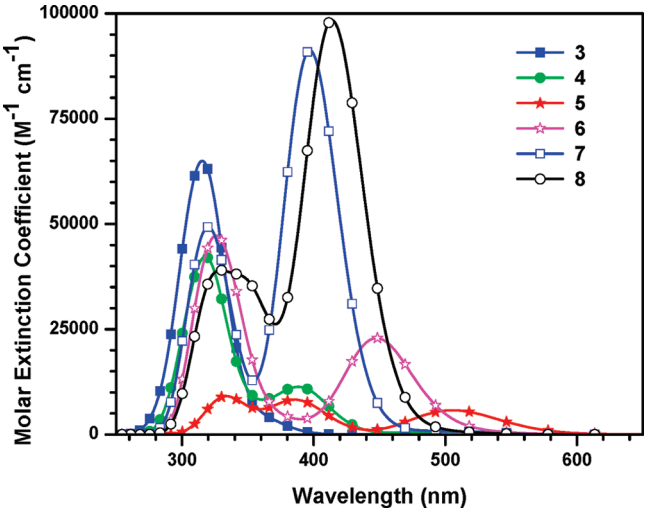

FIGURE 7. Simulated electronic transitions for the compounds (**3**−**8**) using the computed parameters and using mixed Gaussian and Lorentian line shape with an average full-width half-maximum of 3000 cm^{-1} for all transitions.

Consequently, the ionization potential assumes the order **3** > **4** > **5** > **6** > **7** > **8**. The dipole moments calculated for the derivatives in the gas phase are small, and it is possible that the dipole vectors lie in opposite directions and cancel one another.

It is well-known that the HOMOs, LUMOs, and energy gaps are directly related to the optical properties. Vertical transitions for the normal forms of the substituted 6*H*-indolo[2,3-*b*]quinoxaline/arylamine hybrids were calculated by the TDDFT method. The transition energies, oscillator strengths, and assignments for the most relevant singlet excited states in the each molecule are listed in Tables 4, and the simulated spectra from the computed parameters and an average full-width at half-maximum of 3000 cm^{-1} are displayed in Figure 7. The lowest energy transition for the compounds **3**−**6** is in general corresponding to a charge-transfer excitation from the HOMO to the LUMO with smaller oscillator strength. Such a less intense transition is less likely to be observed in the experimental measurements.

However, a slightly intense HOMO to LUMO transition is predicted for the compounds **5** and **6**, which is in good agreement with the parameters experimentally observed for the higher wavelength transitions in these compounds. A considerable red-shift for the theoretical vertical transitions is related to the self-interaction error in TD-DFT arising through the electron transfer in the extended charge-transfer state.[32] The band experimentally found around 320−340 nm in the dyes appears to be composed of multiple overlapping $\pi-\pi^*$ transitions involving HOMO−1 and LUMO+1 orbitals (Table 4). Additionally, the intense $\pi-\pi^*$ transitions realized for the compounds **7** and **8** are emulated well by the theoretical calculations.

Conclusions

We have synthesized a series of indolo[2,3-*b*]quinoxaline-containing triarylamines via palladium-catalyzed C−N/C−C cross-coupling reactions in good yields. The compounds were thoroughly analyzed by routine spectral methods and subjected to photophysical, electrochemical, and thermal studies. The absorption and electrochemical properties of the dyes are significantly influenced by the nature of the diarylamine segment attached to the indole nucleus and their mode of attachment. Insertion of a conjugating aromatic linker between the amine and the indoloquinoxaline units, due to the extended overlap of orbitals, leads to the higher molar extinction coefficients for the absorptions. Crystal structure of compound **6** indicates the lack of $\pi-\pi$ interaction due to the nonplanar triarylamine structural elements despite the presence of flat aromatic segments. However, the weak C−H$\cdots\pi$ interactions present in the molecule may be beneficial for the charge-transporting properties. The emission colors of these materials were tuned from yellow to orange by changing the nature of the amine. Introduction of the indolo[2,3-*b*]quinoxaline moiety in the triarylamine structure leads to red-shifted absorption and emission as well as larger Stokes shift; however, a dramatic decrease in the fluorescence efficiency also occurs. All of the dyes display one single-step, one-electron quasi-reversible oxidation couple in cyclic voltammograms which is attributable to the oxidation of the peripheral amines at the 9-positions of the 6*H*-indolo[2,3-*b*]quinoxaline core, whereas an additional one-electron oxidation process observable at the high positive potentials for the compounds **7** and **8** probably arises from the oxidation of the arylthiophene segment. Introduction of an aromatic spacer between the amine and indoloquinoxaline or extension of the conjugation pathway reduces the band gap as revealed by the theoretical investigations in the gas phase. This observation is beneficial for the adjustment of the HOMO and LUMO without significantly disturbing the optical parameters. There are reasonable correlations between the optical data, electrochemical data, and DFT calculations. Minor deviations may be occur because of the solvent interactions with the dipolar species in solution. The indoloquinoxaline-containing triarylamines display promising thermal stability and higher glass transition temperatures when compared to the similar compounds containing biphenyl or fluorene moieties. However, the low emission yield observed for these dyes highlights the dominance of nonradiating pathways leading to the quenching of the excited state. Though the triarylamines derived from indoloquinoxaline reported here may not be directly applied in emission-based devices, the structure−property relationship revealed from the current investigation highlights the importance of their charger-transfer character. This can be tuned by appropriate functionalization, and the resulting materials may be exploited for application in devices which require significant charge separation. We are currently working in the direction of developing organic dyes containing indoloquinoxaline segments suitable for applications in excitonic solar cells.

(32) (a) Elangovan, A.; Kao, K.-M.; Yang, S.-W.; Chen, Y.-L.; Ho, T.-I.; Su, Y. O. *J. Org. Chem.* **2005**, *70*, 4460. (b) Marsden, J. A.; Miller, J. J.; Shirtcliff, L. D.; Haley, M. M. *J. Am. Chem. Soc.* **2005**, *127*, 2464.

Experimental Section

General Methods. ^{1}H and ^{13}C spectra were recorded on either a 400 or 500 MHz spectrometer. Mass spectra were collected on an ESI TOF high-resolution mass spectrometer. Electronic absorption spectra were measured on a spectrometer using dichloromethane or toluene solutions. Emission spectra were recorded using a spectrofluorimeter operating at room temperature (~32 °C). Emission quantum yields were obtained by using coumarin-6 (Φ_F = 0.78 in ethanol) as reference. Cyclic voltammetry experiments were performed using an electrochemical analyzer with a conventional three-electrode configuration consisting of a glassy carbon working electrode, platinum auxiliary electrode, and a nonaqueous $Ag/AgNO_3$ reference electrode. The $E_{1/2}$ values were determined as $1/2(E^p_a + E^p_c)$, where E^p_a and E^p_c are the anodic and cathodic peak potentials, respectively. All potentials reported are not corrected for the junction potential. The solvent in all experiments was CH_2Cl_2, and the supporting electrolyte was 0.1 M tetrabutylammonium hexafluorophosphate. DSC measurements were carried out on a differential scanning calorimeter at a heating rate of 10 °C/min and a cooling rate of 30 °C/min under nitrogen atmosphere. TGA measurements were performed on a thermogravimetric analyzer at a heating rate of 10 °C/min under a flow of air.

6-Butyl-6*H*-indolo[2,3-*b*]quinoxaline (1). In a round-bottom flask (250 mL), 6*H*-indolo[2,3-*b*]quinoxaline (6.57 g, 30 mmol) and BTEAC (1 g) were suspended on an alkali solution (11 g of NaOH in 30 mL water). It was flushed with nitrogen, and benzene (10 mL) and 1-bromobutane (5.71 mL, 60 mmol) were added in that order via a syringe. The reaction mixture was thoroughly stirred while being heated at 60 °C using an oil bath for 12 h. The reaction was quenched by pouring into hot water, and volatiles were slowly evaporated in a well ventilated hood, overnight. The red solid resulted was filtered and washed with a large amount of water. The desired green emitting compound was purified by column chromatography on silica gel by elution with a 1:8 dichloromethane−hexane mixture. A lemon yellow solid weighing 6.3 g (77%, 22.8 mmol) was obtained: ^{1}H NMR (500 MHz, $CDCl_3$) δ 0.99 (t, J = 7.0 Hz, 3H), 1.45 (sext, J = 7.5 Hz, 2H), 1.94 (quin, J = 7.5 Hz, 2H), 4.50 (t, J = 7.5 Hz, 2H), 7.38 (t, J = 7.5 Hz, 1H), 7.49 (t, J = 8.0 Hz, 1H), 7.68 (q, J = 7.5 Hz, 2H), 7.77 (t, J = 7.0 Hz, 1H), 8.14 (d, J = 8.5 Hz, 1H), 8.30 (d, J = 8.0 Hz, 1H), 8.49 (d, J = 7.5 Hz, 1H); ^{13}C NMR (125 MHz, $CDCl_3$) δ 13.8, 20.4, 30.6, 41.2, 109.5, 119.5, 120.7, 122.7, 125.9, 127.8, 128.7, 129.3, 130.9, 139.3, 140.0, 140.7, 144.5, 145.7; HRMS calcd for $C_{18}H_{17}N_3$ m/z 275.1422, found 275.1421.

9-Bromo-6-butyl-6*H*-indolo[2,3-*b*]quinoxaline (2). In a round-bottom flask (250 mL) protected from sunlight, 6-butyl-6*H*-indolo[2,3-*b*]quinoxaline (2.75 g, 10.0 mmol) was dissolved in 50 mL of anhydrous dimethylformamide. To this solution was added dropwise *N*-bromosuccinimide (2.14 g, 12.0 mmol) dissolved in 20 mL of dimethylformamide through a dropping

funnel. After the addition, the reaction mixture was stirred at room temperature for 24 h. Finally, the reaction was quenched by addition of ice-cold water. The precipitates formed were filtered and dried under vacuum. TLC indicated the presence of a single component: yellow solid; yield 3.38 g (96%, 9.54 mmol); mp 201 °C; ^{1}H NMR (500 MHz, $CDCl_3$) δ 0.98 (t, J = 7.5 Hz, 3H), 1.40−1.45 (m, 2H), 1.91−1.94 (m, CH_2), 4.48 (t, J = 7.5 Hz, 2H), 7.37 (d, J = 9.0 Hz, 1H), 7.69−7.71 (m, 1H), 7.76−7.79 (m, 2H), 8.14 (dd, J = 7.0 Hz, 1.3 Hz, 1H), 8.28 (dd, J = 7.0 Hz, 1.3 Hz, 1H), 8.61 (d, J = 1.5 Hz, 1H); ^{13}C NMR (125 MHz, $CDCl_3$) δ 13.8, 20.3, 30.5, 41.4, 111.0, 113.5, 121.1, 125.4, 126.2, 127.9, 129.2, 129.4, 133.4, 138.6, 139.4, 140.9, 142.9, 145.5, 162.6; HRMS calcd for $C_{18}H_{16}BrN_3$ m/z 353.0528, found 353.0526.

General C−N Coupling Procedure for the Synthesis of the Diarylamine-Substituted Compounds 3−6. A mixture of 9-bromo-6-butyl-6*H*-indolo[2,3-*b*]quinoxaline (1.77 g, 5 mmol), diarylamine (6 mmol), $Pd(dba)_2$ (0.1 mmol), (t-Bu)$_3$P (0.1 mmol), sodium *tert*-butoxide (7.5 mmol), and toluene (15 mL) taken in a Schlenk tube was heated at 80 °C for 12 h. After completion of the reaction, the volatiles were evaporated to leave an orange residue. The residue was purified by column chromatography by using dichloromethane/hexane mixture (1:2) as eluant. For the compounds **6** and **7**, the initial residue was washed with methanol before column chromatography purification to remove the unreacted diarylamine.

6-Butyl-*N*,*N*-diphenyl-6*H*-indolo[2,3-*b*]quinoxalin-9-amine (3): orange solid; yield 72%; mp 188 °C; ^{1}H NMR (400 MHz, $CDCl_3$) δ 0.99 (t, J = 7.2 Hz, 3H), 1.46 (sext, J = 7.2 Hz, 2H), 1.94 (quin, J = 7.2 Hz, 2H), 4.47 (t, J = 7.2 Hz, 2H), 6.97 (t, J = 7.3 Hz, 2H), 7.10 (d, J = 7.6 Hz, 4H), 7.21−7.25 (m, 4H), 7.39 (d, J = 8.7 Hz, 1H), 7.52 (dd, J = 8.7 Hz, 2.2 Hz, 1H), 7.62 (td, J = 7.2 Hz, 1.4 Hz, 1H), 7.72 (td, J = 8.4 Hz, 1.2 Hz, 1H), 8.10 (dd, J = 8.4 Hz, 1.2 Hz, 1H), 8.19 (dd, J = 8.4 Hz, 1.3 Hz, 1H), 8.26 (d, J = 2.2 Hz, 1H); ^{13}C NMR (125 MHz, $CDCl_3$) δ 13.8, 20.4, 30.7, 41.4, 110.4, 120.1, 120.5, 121.5, 121.7, 122.0, 122.3, 122.5, 122.7, 123.3, 123.3, 123.5, 124.9, 125.9, 126.1, 127.8, 128.0, 128.8, 129.27, 129.29, 129.34, 129.5, 129.7, 139.2, 139.7, 140.7, 141.0, 141.8, 146.1, 147.9, 148.4; HRMS calcd for $C_{30}H_{27}N_4$ (M + H) m/z 443.2236, found 443.2235. Anal. Calcd for $C_{30}H_{26}N_4$: C, 81.42; H, 5.92; N, 12.66. Found: C, 81.57; H, 6.01; N, 12.45.

6-Butyl-*N*-(naphthalen-1-yl)-*N*-phenyl-6*H*-indolo[2,3-*b*]quinoxalin-9-amine (4): orange solid; yield 81%; mp 175 °C; ^{1}H NMR (400 MHz, $CDCl_3$) δ 0.98 (t, J = 7.4 Hz, 3H), 1.44 (sext, J = 7.5 Hz, 2H), 1.92 (quin, J = 7.4 Hz, 2H), 4.44 (t, J = 7.3 Hz, 2H), 6.85 (t, J = 7.3 Hz, 1H), 6.95 (d, J = 7.7 Hz, 2H), 7.15−7.19 (m, 2H), 7.32−7.37 (m, 3H), 7.42−7.48 (m, 2H), 7.51 (dd, J = 8.7 Hz, 2.3 Hz, 1H), 7.60 (td, J = 7.6 Hz, 1.4 Hz, 1H), 7.68 (td, J = 7.7 Hz, 1.5 Hz, 1H), 7.75 (d, J = 8.4 Hz, 1H), 7.87 (d, J = 8.2 Hz, 1H), 8.04 (d, J = 8.4 Hz, 1H), 8.09 (dd, J = 8.4 Hz, 1.0 Hz, 1H), 8.16 (dd, J = 8.3 Hz, 1.2 Hz, 1H) 8.22 (d, J = 2.2 Hz, 1H); ^{13}C NMR (125 MHz, $CDCl_3$) δ 13.7, 20.2, 30.5, 41.1, 110.0, 117.7, 120.1, 120.4, 120.8, 124.2, 126.0, 126.1, 126.3, 126.9, 127.6, 127.7, 128.3, 128.6, 129.0, 131.0, 135.3, 138.9, 139.6, 140.3, 140.5, 142.6, 143.8, 145.9, 149.3; HRMS calcd for $C_{34}H_{29}N_4$ (M + H) m/z 493.2392, found 493.2400. Anal. Calcd for $C_{34}H_{28}N_4$: C, 82.90; H, 5.73; N, 11.37. Found: C, 82.78; H, 5.51; N, 11.26.

***N*-(Anthracen-9-yl)-6-butyl-*N*-phenyl-6*H*-indolo[2,3-*b*]quinoxalin-9-amine (5):** orange solid; yield 76%; mp 238 °C; ^{1}H NMR (400 MHz, $CDCl_3$) δ 1.01 (t, J = 7.4 Hz, 3H), 1.48 (sext, J = 7.6 Hz, 2H), 1.96 (quin, J = 7.4 Hz, 2H), 4.49 (t, J = 7.3 Hz, 2H), 7.05 (t, J = 7.3 Hz, 1H), 7.16 (d, J = 8.1 Hz, 2H), 7.29−7.38 (m, 5H), 7.42−7.47 (m, 2H), 7.59−7.63 (m, 2H), 7.70−7.74 (td, J = 6.9 Hz, 1.2 Hz, 1H), 7.82−7.88 (m, 2H), 7.92−7.94 (m, 1H), 8.07 (s, 1H), 8.12 (d, J = 8.5 Hz, 1H), 8.18 (d, J = 8.4 Hz, 1H) 8.30−8.34 (m, 2H); ^{13}C NMR (125 MHz, $CDCl_3$) δ 13.7, 20.2, 30.6, 41.2, 110.3, 117.2, 120.2, 122.7, 123.8, 124,1, 124.2, 124.4, 125.75, 125.81, 127.5, 127.6, 128.0, 128.6, 129.0, 129.2, 129.7, 130.6, 132.0, 132.5, 139.0, 139.5, 140.6, 141.1, 141.3, 145.2, 147.8; HRMS calcd for $C_{38}H_{31}N_4$ (M + H) m/z 543.2549, found 543.2549. Anal. Calcd for $C_{38}H_{30}N_4$: C, 84.10; H, 5.57; N, 10.32. Found: C, 83.87; H, 5.43; N, 10.18.

6-Butyl-*N*-phenyl-*N*-(pyren-2-yl)-6*H*-indolo[2,3-*b*]quinoxalin-9-amine (6): red solid; yield 85%; mp 161 °C; ^{1}H NMR (400 MHz, $CDCl_3$) δ 0.97 (t, J = 7.4 Hz, 3H), 1.43 (sext, J = 7.6 Hz, 2H), 1.91 (quin, J = 7.5 Hz, 2H), 4.43 (t, J = 7.3 Hz, 2H), 6.92 (t, J = 7.3 Hz, 1H), 7.02 (dd, J = 8.7 Hz, 1.0 Hz, 2H), 7.15−7.21 (m, 2H), 7.34 (d, J = 8.7 Hz, 1H), 7.55−7.60 (m, 2H), 7.68−7.70 (m, 1H), 7.88 (d, J = 8.2 Hz, 1H), 7.91−7.98 (m, 2H), 8.04 (s, 2H), 8.07−8.10 (m, 2H), 8.14−8.17 (m, 3H) 8.25 (d, J = 9.2 Hz, 1H). 8.29 (d, J = 2.2 Hz, 1H); ^{13}C NMR (125 MHz, $CDCl_3$) δ 13.8, 20.3, 30.7, 41.3, 110.3, 117.9, 120.3, 120.8, 121.1, 123.4, 124.9, 125,0, 125.2, 126.1, 126.2, 126.5, 127.0, 127.2, 127.5, 127.88, 127.92, 128.7, 129.0, 129.2, 129.3, 129.4, 131.1, 131.3, 139.0, 139.7, 140.4, 140.7, 141.3, 142.9, 146.0, 149.6; HRMS calcd for $C_{40}H_{31}N_4$ (M + H) m/z 567.2549, found 567.2550. Anal. Calcd for $C_{40}H_{30}N_4$: C, 84.78; H, 5.34; N, 9.52. Found: C, 84.61; H, 5.21; N, 9.65.

4-(5-(6-Butyl-6*H*-indolo[2,3-*b*]quinoxalin-9-yl)thiophene-2-yl)-*N*,*N*-diphenylaniline (7). To a mixture of 9-bromo-6-butyl-6*H*-indolo[2,3-*b*]quinoxaline (1.77 g, 5 mmol), *N*,*N*-diphenyl-4-(5-(tributylstannyl)thiophene-2-yl)aniline[23] (3.7 g, 6 mmol), and dry dimethylformamide (10 mL) was added $Pd(PPh_3)_2Cl_2$ (35 mg) and the mixture heated at 70 °C for 17 h. After the reaction was over, the orange suspension was cooled, and methanol (30 mL) was added to complete the precipitation. It was filtered and the residue dried. The crude product was purified by column chromatography on silica gel by using a hexane/dichloromethane mixture (2:1) as eluant: orange solid; yield 4.56 (76%); mp 218 °C; ^{1}H NMR (400 MHz, $CDCl_3$) δ 0.98 (t, J = 7.4 Hz, 3H), 1.42 (sext, J = 7.5 Hz, 2H), 1.92 (quin, J=7.4 Hz, 2H), 4.49 (t, J=7.2 Hz, 2H), 7.01−7.13 (m, 9H), 7.22−7.28 (m, 7H), 7.35 (d, J=3.7 Hz, 1H), 7.45−7.51 (m, 3H), 7.67 (td, J = 7.6 Hz, 1.3 Hz, 1H), 7.75 (td, J = 7.4 Hz, 1.4 Hz, 1H), 7.94 (dd, J = 8.5 Hz, 1.7 Hz, 1H), 8.13 (dd, J = 7.9 Hz, 1.0 Hz, 1H) 8.30 (dd, J = 8.3 Hz, 1.1 Hz, 1H). 8.72 (d, J= 1.3 Hz, 1H); ^{13}C NMR (125 MHz, $CDCl_3$) δ 13.9, 20.4, 30.7, 41.3, 100.0, 119.3, 119.9, 123.3, 123.3, 123.6, 123.7, 124.6, 126.1, 126.3, 127.64, 127.9, 128.4, 128.5, 128.9, 129.4, 139.3, 139.8, 140.8, 142.7, 143.0, 143.5, 145.9, 147.2; HRMS calcd for $C_{40}H_{33}N_4S$ (M + H) m/z 601.2426, found 601.2421. Anal. Calcd for $C_{40}H_{32}N_4S$: C, 79.97; H, 5.37; N, 9.33. Found: C, 79.63; H, 5.31; N, 9.12.

8-(5-(6-Butyl-6*H*-indolo[2,3-*b*]quinoxalin-9-yl)thiophene-2-yl)-9,9-diethyl-*N*,*N*-diphenyl-9*H*-fluoren-1-amine (8). Compound **8** was obtained in 79% yield as a red solid from 9,9-diethyl-*N*,*N*-diphenyl-7-(5-(tributylstannyl)thiophene-2-yl)-9*H*-fluoren-2-amine[25] and 9-bromo-6-butyl-6*H*-indolo[2,3-*b*]quinoxaline as described above: mp 195 °C; ^{1}H NMR (400 MHz, $CDCl_3$) δ 0.41 (t, J = 7.3 Hz, 3H), 0.98 (t, J = 7.4 Hz, 3H), 1.44 (sext, J = 7.6 Hz, 2H), 1.91−2.02 (m, 6H), 4.48 (t, J = 7.2 Hz, 2H), 6.98−7.05 (m, 3H), 7.10−7.14 (m, 5H), 7.23−7.27 (m, 4H), 7.36−7.39 (m, 2H), 7.46 (d, J = 8.5 Hz, 1H), 7.55−7.57 (m, 2H), 7.61 (s, 2H), 7.65−7.73 (m, 1H), 7.73−7.77 (m, 1H), 8.12−8.14 (dd, J = 8.4 Hz, 1.2 Hz, 1H) 8.29−8.32 (dd, J = 8.4 Hz, 1.3 Hz, 1H). 8.74 (d, J = 1.8 Hz, 1H); ^{13}C NMR (125 MHz, $CDCl_3$) δ 8.5, 13.7, 20.2, 30.5, 32.6, 41.2, 56.0, 109.8, 119.15, 119.21, 119.3, 119.6, 119.8, 120.2, 122.4, 123.6, 123.7, 124.4, 125.9, 127.5, 127.7, 128.5, 128.8, 129.4, 129.2, 132.2, 136.0, 139.2, 139.7, 140.6, 140.8, 142.8, 143.5, 143.8, 145.8, 147.1, 147.8, 150.5, 151.4; HRMS calcd for $C_{51}H_{45}N_4S$ (M + H) m/z 745.3365, found 745.3371. Anal. Calcd for $C_{51}H_{44}N_4S$: C, 82.22; H, 5.95; N, 7.52. Found: C, 81.97; H, 5.81; N, 7.36.

Computational Methods. The ground-state geometry of the compounds at the gas phase were optimized using the density functional theory method with the B3LYP functional in conjugation with the basis set 6-31G(d,p) as implemented in the Gaussian 09 package.[29] The default options for the self-consistent field (SCF) convergence and threshold limits in the optimization were used. The electronic transitions were calculated using the time-dependent DFT (B3LYP) theory and the 6-31G

(d,p) basis set. Even though the time-dependent DFT method less accurately describes the states with charge-transfer nature, the qualitative trends in the TDDFT results can still offer correct physical insights. At least 10 excited states were calculated for each molecule.

Crystallographic Measurements. Red crystals of **6** were grown from CH_2Cl_2/*n*-hexane at room temperature. Data collection was carried out on Kappa APEX 11 and Bruker AXS single-crystal X-ray diffractometers at room temperature. Mo Kα radiation (λ = 0.71073 Å) was used. The unit-cell parameters were obtained by least-squares fit to the automatically centered settings for reflections. Data were collected in $\omega/2\theta$ scan mode. Corrections were made for Lorentz and polarization effects. All calculations were performed using the WINGX software package. Structure solution was done by direct methods and refined by a full-matrix least-squares method on F^2 (F = structure factor). The monoclinic space group $P12_1/n1$ was determined from the systematic absence of specific reflections; successful refinement of the structure confirmed the space group assignment. The dichloromethane solvent present in the crystal and the butyl fragment were found to be disordered, and this explains the observed high R values.

Acknowledgment. We thank the Department of Science and Technology (DST), New Delhi, India, for financial support (Grant No. SR/S1/OC-11/2007). The single-crystal X-ray facility at the Sophisticated Analytical Instrumentation Facility of the Indian Institute of Technology, Madras, is also acknowledged for X-ray diffraction data collection. Prof. R. Barthwal of the Department of Biotechnology is thanked for allowing us to use the NMR facility in the Institute Instrumentation Centre.

Supporting Information Available: ^{1}H and ^{13}C NMR and HR mass spectra of the newly synthesized compounds, crystallographic data for the compound **6**, and Cartesian coordinates of the optimized structures. This material is available free of charge via the Internet at http://pubs.acs.org.

Note Added after ASAP Publication. In the version published asap November 5, 2010, compound **6** in Chart 1 is depicted with a wrong connectivity; the correct version reposted November 11, 2010.